Misfit relaxation of $La_{0.7}Sr_{0.3}MnO_3$ thin films by a nanodot segregation mechanism

P. Abellán,[1] C. Moreno,[1] F. Sandiumenge,[1,a)] X. Obradors,[1] and M.-J. Casanove[2]
[1]*Institut de Ciència de Materials de Barcelona, CSIC, Campus de la Universitat Autònoma de Barcelona, Bellaterra, Catalonia 08193, Spain*
[2]*Centre d'Elaboration des Materiaux et d'Etudes Structurales, CNRS, BP 4347, 29 rue J. Marvig, F-31055 Toulouse Cedex 4, France*

(Received 5 November 2010; accepted 6 January 2011; published online 25 January 2011)

Partially segregated $La_{0.7}Sr_{0.3}MnO_3$ (LSMO) nanocomposite films are shown to exhibit a thickness dependent self-assembled structure. The morphological evolution of the nanocomposite and the misfit strain of the LSMO phase are linked through the topological distribution of La–Sr oxide nanodots within the film. Misfit relaxation occurs above a critical thickness, h_c, coinciding with the nucleation of La–Sr oxide nanodots at the film-substrate interface. Below h_c, the same dots outcrop the film surface, forming islands. As a consequence of this misfit relaxation mechanism, an enhancement in the magnetoresistance with increasing thickness is measured. © *2011 American Institute of Physics*. [doi:10.1063/1.3549182]

The ability to assemble multiphase materials at the nanoscale constitutes a cornerstone to the realization of novel functionalities. Among different approaches, the simultaneous growth of two epitaxial phases leading to a three dimensional assembling of one crystal embedded in another is nowadays receiving much attention in a variety of functional/multifunctional oxide systems.[1–4] These studies reveal that structural compatibility[1,2] and interface energy[4] constitute the major parameters governing the topological pattern of the resulting nanostructures.

As an alternative approach, it has been recently shown that thin $La_{0.7}Sr_{0.3}MnO_3$ (LSMO) films subjected to specific nonequilibrium conditions undergo a self-assembled segregation mechanism of La–Sr oxide (LSO) islands of unknown crystal structure and $Sr_3Mn_4O_7$ Ruddelsden–Popper (RP) type inclusions in a way that the simultaneous formation of both phases maintains the LSMO stoichiometry and rhombohedral structure unaltered.[5] In this work, we present an investigation of the interplay between the misfit relaxation of LSMO films and the topological distribution of spontaneously segregated LSO nanodots. According to the dislocation model,[6] LSMO films grown on $SrTiO_3$ (STO) would relax at a critical thickness $h_c \sim 10-12$ nm,[7,8] in strong disagreement with experimental values lying above 100 nm.[9–13] In contrast to this behavior, here we show that partially segregated nanocomposite films relax at a much lower thickness, ~60 nm, than nonsegregated ones. This behavior is associated with a different localization of the LSO phase from outcropping islands to film-substrate interfacial nanodots.

Segregated $La_{0.7}Sr_{0.3}MnO_3$ thin films with thicknesses of 24, 35, and 60 nm were prepared by metal-organic decomposition as described elsewhere.[5] Their structure was analyzed by x-ray diffraction and transmission electron microscopy (TEM) using a JEM-2011 and a spherical aberration corrected Tecnai F20 electron microscopes at 200 kV. Transport properties were measured in lithographed films by the four point technique using a Quantum Design physical property measurement system.[14] Figure 1 shows that the thinnest film (a) has LSO islands, while the thickest one exhibits a flat surface and LSO nanodots embedded at the LSMO-STO interface (b). During the segregation of LSO, the stoichiometry of the LSMO film is balanced by the simultaneous formation of bulk RP inclusions[5] [see inset in Fig. 1(a)]. In contrast to LSO, the topological distribution of RP inclusions is not film thickness dependent. On the other hand, reciprocal space mapping analysis [see Fig. 2(a)] shows that the separation between the (103)-LSMO and (103)-STO peaks evolves with thickness according to a progressive misfit relaxation. The thickness dependence of the film in-plane and out-of-plane lattice parameters indicates that almost complete relaxation is achieved at 60 nm (d). Therefore, the relaxation of partially segregated films occurs at a smaller thickness (~60 nm) than nonsegregated ones (>100 nm, see Refs. 9–12), coinciding with a topological redistribution of the LSO phase from the film surface to the film-substrate interface.

This result suggests that interfacial LSO decisively contributes to the misfit relaxation of the LSMO composite film. The matching distances along the *pseudo*cubic unit cell in-plane and out-of-plane parameters of LSMO, determined for the LSO islands, are $d_{\parallel} \sim d_{\perp} \sim 0.405$ nm $> a_{STO}$ (Ref. 5) [$a_{STO} = 0.3905$ nm (Ref. 15)]. As a consequence, the LSMO film is tensile strained around the nanodots to a larger extent

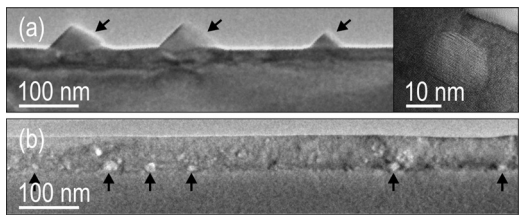

FIG. 1. Comparison of cross sectional TEM views along the [100] direction of the LSMO and the STO for the 24 nm (a) and 60 nm (b) films. The thinnest film contains LSO islands (a), in contrast to the thickest one where the LSO phase forms nanodots at the STO-LSMO interface (b). The inset in (a) shows an example of a RP inclusion. Such inclusions remain in the bulk in thicker films.

a)Author to whom correspondence should be addressed. Electronic mail: felip@icmab.es.

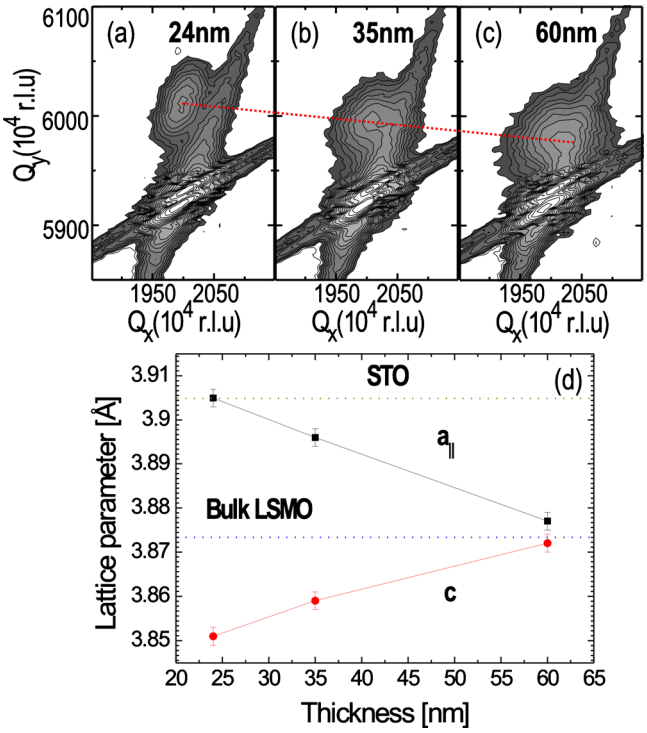

FIG. 2. (Color online) Thickness dependence of the in-plane and out-of-plane LSMO lattice parameters. The reciprocal space maps around the (103) reflections of LSMO and STO for the 24 nm (a), 35 (nm), and 60 nm (c) thick LSMO films indicate misfit relaxation with increasing film thickness. The thickness dependence of the lattice parameters shows an almost complete relaxation for a thickness of 60 nm (d). rlu means "reciprocal lattice units" and 1 rlu=$2/\lambda$ with λ=0.541 84 nm.

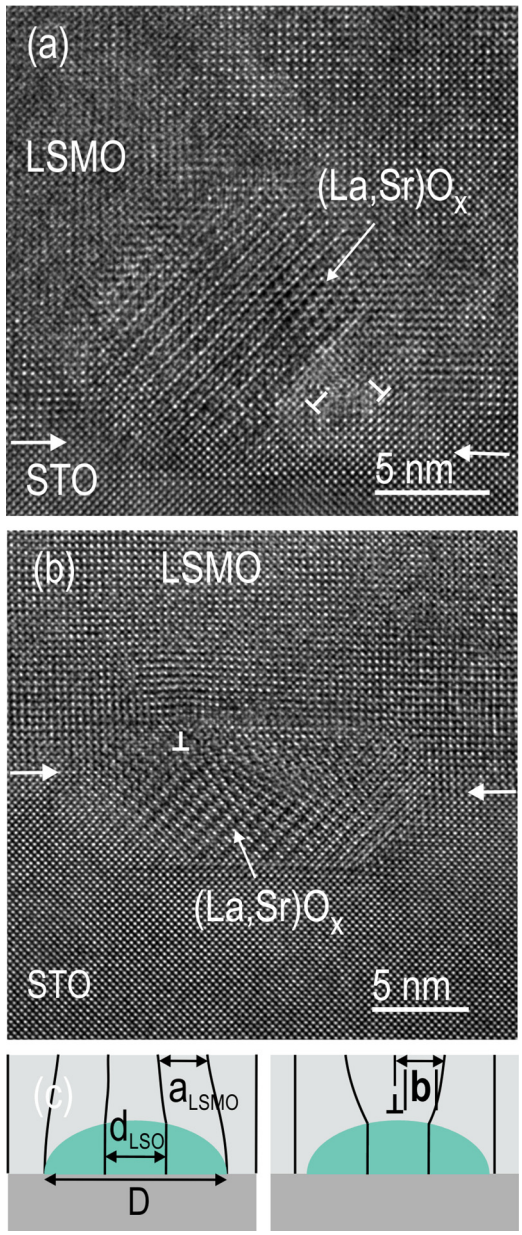

FIG. 3. (Color online) High resolution TEM images of LSO interfacial nanodots in the 60 nm film. One lying on top of the substrate (a) and one partially embedded in the substrate (b). The nanodots exhibit a high degree of interfacial coherency with their embedding LSMO and STO perovskite structures. In both cases, misfit dislocations are formed, contributing to the relaxation of the LSMO film. (c) Schematic drawing illustrating the misfit accommodation mechanism by interfacial nanodots.

than at the LSMO/STO interface [a_{LSMO}=0.3876 nm (Ref. 16)]. Therefore, the 0.7% tensile misfit at the film-substrate interface can be partially relieved by the interfacial nucleation of LSO nanodots whenever the sum of their strain and interfacial energies is smaller than the concomitant reduction in misfit elastic strain energy. Figure 3 shows examples of interfacial nanodots [(a) and (b)] along with a schematic drawing of the misfit accommodation mechanism (c). The nanodots are faceted along the $\{100\}_{LSMO}$ and $\{110\}_{LSMO}$ perovskite planes, suggesting local minima in the interface energy for these orientations.[17,18] Strikingly, in (b) the LSO nanodot is partially embedded in the STO substrate. The mechanism leading to this configuration is not clearly understood. The lateral displacement induced in the neighboring LSMO lattice by a LSO nanodot is $B=\varepsilon^{LSMO/LSO}\cdot D$ [D is the diameter of the nanodot projected onto the interface and $\varepsilon^{LSMO/LSO}=(d_{LSO}-a_{LSMO})/a_{LSMO}$]. Thus, a nanodot with size $D_{eq}=|\mathbf{b}|/\varepsilon^{LSMO/LSO}$ induces a compensating strain around it equivalent to a misfit dislocation with Burgers vector $\mathbf{b}$. Quantitative analysis of the images using the geometrical phase analysis method[19] indicated that the matching distances of interfacial LSO are smaller than those of LSO islands, yielding displacements of $B\sim0.48$ nm and ~0.23 nm for (a) and (b), respectively.

It should be pointed out that the misfit compensating effect of interfacial nanodots is only efficient within a slab of LSMO adjacent to the interface. Analysis of the high resolution TEM images shown in Figs. 3(a) and 3(b) indicates, however, that once nucleated, such nanodots constitute preferential nucleation sites for dislocations with Burgers vectors $\mathbf{b_1}=a_{LSMO}/2[0\bar{1}\bar{1}]$ and $\mathbf{b_2}=a_{LSMO}/2[0\bar{1}1]$, yielding misfit components $\mathbf{b_1}+\mathbf{b_2}=a_{LSMO}[100]$ [Fig. 3(a)] and $\mathbf{b}=a_{LSMO}[100]$ [Fig. 3(b)], with the extra plane residing in the LSMO film. Such dislocations compensate (totally or partially) the displacement B induced by the nanodots, thus relaxing the misfit strain through the entire volume of the composite film. Note that beyond a size corresponding to $B>|\mathbf{b}|$, the cost in elastic and interface energies for interfacial nucleation would be no longer compensated by a reduction of the film elastic strain energy, thus explaining the observed large discrepancy between the island and nanodot sizes.

Contrary to the typical behavior of manganite thin films,[20,21] no thickness or strain dependence of the Curie temperature, $T_C\sim360$ K, was observed in this study. Nevertheless, the residual resistivity at 5 K (inset in Fig. 4) is

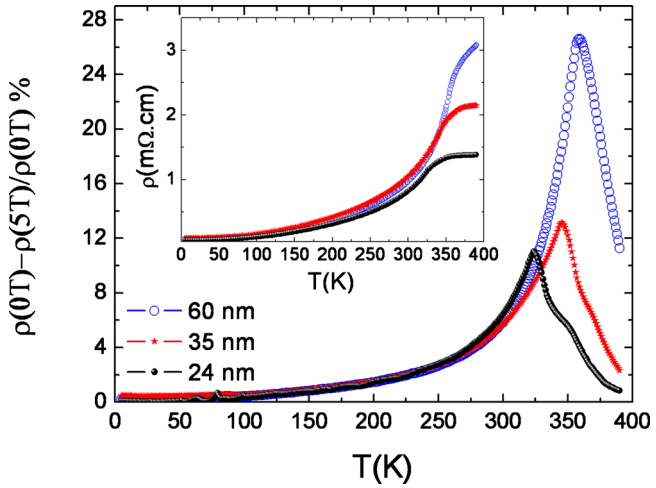

FIG. 4. (Color online) Transport properties of LSMO films. Magnetoresistance at 5 T and temperature dependence of the resistivity (inset) for the 24, 35, and 60 nm films. The metal-insulator transition temperature, T_{MI}, is determined as the maximum in the differential resistivity in the $\rho(T)$ curve.

similar to that previously reported for $La_{0.7}Sr_{0.3}MnO_3$ single crystal films[22] ($<10^{-4}$ Ω cm), confirming the high quality of the present LSMO composite samples. The metal-insulator transition temperature, T_{MI} (see Fig. 4) decreases, while the magnetoresistance peak broadens and moves to lower temperatures as the films become more strained. The maximum magnetoresistance increases from 11% at 24 nm to 27% at 60 nm. Notably, magnetoresistance (MR) increases by more than a factor of 2 without decreasing T_C. This differential behavior can be associated with local nanostrain variations induced around the interfacial LSO and bulk RP inclusions. This structural disorder is reflected in the reciprocal space maps as a broadening of the (103) film reflection (see Fig. 2) and is further evidenced by an increase in the high temperature resistivity ($\rho^{390\ K}$).

In summary, a misfit relaxation mechanism based on a thermodynamically induced self-assembled segregation of secondary phases has been investigated for LSMO thin films. In particular, the thickness dependence of MR and $\rho^{390\ K}$ evidences a structural and chemical disorder in the relaxed films that can be correlated with the particular relaxation mechanism described in this work.

We acknowledge the financial support from MEC (CONSOLIDER NANOSELECT, Grant No. MAT2008-01022; FPU), Generalitat de Catalunya (Pla de Recerca, Grant No. 2009-SGR-770, and XaRMAE). The Cs-corrected Tecnai-F20 FEI electron microscope was used in the framework of the European project ESTEEM (Contract No. 026019).

[1]H. Zheng, J. Wang, S. E. Lofland, Z. Ma, L. Mohaddes-Ardabili, T. Zhao, L. Salamanca-Riba, S. R. Shinde, S. B. Ogate, D. Viehland, Y. Jia, D. G. Schlom, M. Wutting, A. Roytburd, and R. Ramesh, Science **303**, 661 (2004).
[2]J. L. MacManus-Driscoll, P. Zerrer, H. Wang, H. Yang, J. Yoon, A. Fouched, R. Yu, M. G. Blamire, and Q. X. Jia, Nature Mater. **7**, 314 (2008).
[3]V. Moshnyaga, B. Damaschke, O. Shapoval, A. Belenchuk, J. Faupel, O. I. Lebedev, J. Verbeeck, G. Van Tendeloo, M. Mücksch, V. Tsurkan, R. Tidecks, and K. Samwer, Nature Mater. **2**, 247 (2003).
[4]H. Zheng, Q. Zhan, F. Zavaliche, M. Sheburne, F. Straub, M. P. Cruz, L.-Q. Chen, U. Dahmen, and R. Ramesh, Nano Lett. **6**, 1401 (2006).
[5]C. Moreno, P. Abellán, A. Hassini, A. Ruyter, A. P. Del Pino, S. Sandiumenge, M.-J. Casanove, J. Santiso, T. Puig, and X. Obradors, Adv. Funct. Mater. **19**, 2139 (2009).
[6]J. W. Matthews, J. Vac. Sci. Technol. **12**, 126 (1975).
[7]J. P. Contour, A. Abert, and A. Défossez, Proc. SPIE **2697**, 339 (1996).
[8]P. Abellán, F. Sandiumenge, C. Moreno, M. J. Casanove, T. Puig, and X. Obradors, Mater. Res. Soc. Symp. Proc. **1174**, V04-12 (2009).
[9]L. Ranno, A. Llobet, R. Tiron, and E. Favre-Nicolin, Appl. Surf. Sci. **188**, 170 (2002).
[10]M.-J. Casanove, P. Baulès, J. Majimel, J.-C. Ousset, D. Magnoux, and J. F. Bobo, Appl. Surf. Sci. **188**, 19 (2002).
[11]J. L. Maurice, F. Pailloux, A. Barthélémy, O. Durand, D. Imhoff, R. Lyonnett, A. Rocher, and J.-P. Contour, Philos. Mag. A **83**, 3201 (2003).
[12]O. I. Lebedev, G. Van Tendeloo, S. Amelinckx, H. L. Hu, and K. M. Krishnan, Philos. Mag. A **80**, 673 (2000).
[13]M. J. Zhuo, Y. L. Zhu, and X. L. Ma, Philos. Mag. Lett. **86**, 469 (2006).
[14]C. Moreno, C. Munuera, A. Perez del Pino, J. Gutiérrez, T. Puig, C. Ocal, and X. Obradors, Phys. Rev. B **80**, 094412 (2009).
[15]J. Brous, I. Fankuchen, and E. Banks, Acta Crystallogr. **6**, 67 (1953).
[16]M. C. Martin, G. Shirane, Y. Endoh, K. Hirota, Y. Morimoto, and Y. Tokura, Phys. Rev. B **53**, 14285 (1996).
[17]K. C. Russell, Adv. Colloid Interface Sci. **13**, 205 (1980).
[18]A. P. Sutton and R. W. Balluffi, *Interfaces in Crystalline Materials* (Clarendon, Oxford, 1995).
[19]M. J. Hÿtch, E. Snoeck, and R. Kilaas, Ultramicroscopy **74**, 131 (1998).
[20]M. Ziese, H. C. Semmelhack, K. H. Han, S. P. Sena, and H. J. Blythe, J. Appl. Phys. **91**, 9930 (2002).
[21]A. J. Millis, T. Darling, and A. Migliori, J. Appl. Phys. **83**, 1588 (1998).
[22]A. Urushibara, Y. Morimoto, T. Arima, A. Asamitsu, G. Kido, and Y. Tokura, Phys. Rev. B **51**, 14103 (1995).